RSC Advances

ROYAL SOCIETY OF CHEMISTRY

www.rsc.org/advances

Graphical Abstract

The effects of cellulose I and cellulose II on the microfibrillation process and final properties of MFC were studied

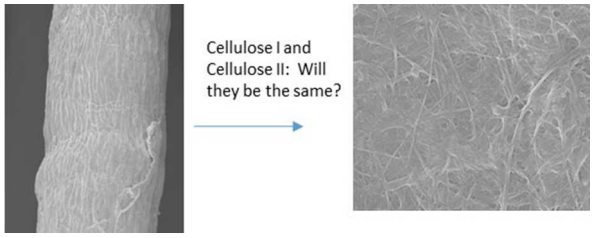

Characterization of micro fibrillation process of cellulose and mercerized cellulose pulp

Sudhir Sharma[a], Sandeep Sudhakaran Nair[b], Zhe Zhang[a], Arthur J. Ragauskas[b], Yulin Deng[a]

a: Georgia Institute of Technology, School of Chemical and Biomolecular Engineering, 311 Ferst Drive NW, Atlanta, GA – 30332

b: Georgia Institute of Technology, School of Chemistry and Biochemistry, 901 Atlantic Drive, Atlanta, GA - 30332

Abstract

Here we detail the fibrillation process for cellulose and mercerized cellulose pulps. Native and mercerized cellulose showed high degree of purity as indicated by α – cellulose content measurement and XRD analysis. Furthermore, stark change in fiber morphology indicated aggregation of fibrils on the surface due to mercerization. Fibrillation of pulp was carried out in the in the following subsequent steps: Disintegration, PFI refining, microgrinding by 20 passes in SuperMassColloider, and 60 passes in SuperMassColloider. Fiber samples were collected at every stage and highly uniform films were made by ultrafiltration and hot press method. The fibers and films made from fibers were then characterized by measuring physical properties, contact angle, thermal, mechanical, and SEM analysis. The main objective was to characterize the physical properties of the films made from different degrees of fibrillation. The films obtained were of fairly close grammage approximately 35g/m^2. The target grammage was 40g/m^2, and the slightly lower grammage indicated some fiber loss during the fabrication process. Additionally, it was observed that the density of the films increased with increasing degree of fibrillation from about 180g/m^3 to 455g/m^3 for cellulose I and 95g/m^3 to 385g/m^3 for cellulose II. Cellulose I films showed some contact angle to begin with which increased at every stage (14° - 64°), whereas cellulose II films did not display a contact angle until the final stage of fibrillation. The films also showed increasing strength and an evolution of tensile strength from initially displaying a tear behavior indicating poor bonding to typical micro fibrillated cellulose films behavior as the fibers became increasingly fibrillated. The ultimate tensile strength for cellulose changed from tear behavior with no defined break to 134.5MPa. While on the other hand, the same change for cellulose II was a maximum of 75.1MPa from tear behavior. Increasing fibrillation of fibrils in both cases showed a decrease in fiber size, well differentiated for the two types of pulps at every stage.

Keywords: Cellulose, micro fibrillated cellulose, nano cellulose, microgrinding, mercerization

1. Introduction

Cellulose is the most abundant, renewable bio polymer on earth, naturally occurring in a variety of sources [1, 2]. Recently the production and potential application of micro fibrillated cellulose fibers have garnered much attention due to their excellent mechanical properties,

biodegradability, and renewability. In the scientific literature, there are reports of various applications of micro fibrillated cellulose based materials including, composites, barrier materials, tissue scaffolds, cell growth media, electronic materials, solar cells, and super capacitors [3-10]. Nanofibers from native cellulose-I have been made using a variety of chemical, mechanical, and enzymatic treatment methods. These include high pressure mechanical homogenization, TEMPO ((2,2,6,6-Tetramethylpiperidin-1-yl)oxyl) oxidation, and enzymatic hydrolysis amongst a host of other methods [9, 11-13].

Four polymorphs of crystalline cellulose-I, II, III, and IV are known, and out of these, cellulose-I and II are the most widely studied. Cellulose-I is known as native cellulose, and is the one found abundantly in nature. Cellulose-I can be converted easily to cellulose-II via mercerization or regeneration processes [14]. Interest in cellulose-II fibers arises because they have a monoclinic structure which is a thermodynamically more stable structure. While the intra sheet bonding structure is essentially the same as cellulose-I, there is also the possibility of formation of additional inter – sheet hydrogen bonds providing the structure with additional stability. In the regeneration process native cellulose fibers are solubilized in a solvent and then re-precipitated in water as cellulose-II. However, that disrupts the fibrous and crystalline structure of the cellulose resulting in poor mechanical properties of the resulting cellulose-II fibers [15, 16]. Mercerization entails swelling the native fibers in a concentrated NaOH solution and then washing off the excess solution after conversion into cellulose-II. Since the fibers are not solubilized, the crystal and fibrous structure of the cellulose remains intact. Thus, mercerization is preferred over regeneration [14, 17-19].

Various authors have previously studied in depth the crystalline, structural and chemical changes of cellulose fibers upon mercerization. Upon mercerization, there is a loss of hemicelluloses, a reduction in degree of polymerization, and change in the crystal structure of the resulting cellulose due to rearrangement of the crystalline parts. Due to these chemical and structural changes, the resulting physical properties of pulp and films made from the pulp should show significant differences in behavior[15, 16, 19-24]. Moreover, due to the seemingly different fiber structure and easy conversion into cellulose-II, it would be conducive to study the characteristics of cellulose-II nanofibers as well. Fibrillated cellulose-I fibers have been subjected to mercerization and characterization before. However, cellulose-II nanofibers obtained from mercerization of cellulose-I nanofibers resulted in irregular aggregation, and an undispersed suspension [15, 16, 19, 25]. These aggregates cannot be re-dispersed effectively again to the nano fibril suspension as is the case for cellulose I.

Given these previously observed issues and the relatively small body of literature on cellulose-II nanofibers; it is imperative to understand the physical process of fibrillation of cellulose-II fibers to form nanofibers. This characterization would help in understanding and elucidating the physical, chemical, and morphological evolution of properties of cellulose-II fibers as they undergo fibrillation to nanofibers, and help to design strategies to optimally produce cellulose-II nanofibers for potential applications. In particular we would elucidate the structure property

relationships for films made from fibrils at different stages of fibrillation for both cellulose I and II. For this study, commercially available bleached softwood pulp was used as starting material. Cellulose-II fiber pulp was prepared from the raw material via mercerization of cellulose-I native cellulose pulp. Subsequently cellulose-I pulp was also subjected to the same processes for characterization to elucidate the differences in evolution of physical properties of the two materials.

2. Experimental

2.1 Materials

Commercially available elementally chlorine free, bleached loblolly pine (softwood) pulp was used as a starting material.

2.2 Pulp mercerization

The pulp was soaked in deionized water for 24 hours to form slurry with 2% consistency. After 24 hours of soaking the pulp was mercerized by soaking adding in an excess of 20% NaOH solution to the slurry. After 24 hours, the slurry was washed with a 1% acetic acid solution to remove any excess NaOH, and subsequently washed with deionized water and adjusted to a consistency of ~2% for further processing.

2.3 α-Cellulose content

α - Cellulose content of both types of cellulose was quantified by dissolution in 17.5% NaOH solution. The method as described by Wang et al[15] was used. Particularly, 1 gram of the dried sample was soaked in 17.5% NaOH solution at 20°C for 45 minutes. After this period, the sample was filtered through a filter glass, and subsequently washed thoroughly with distilled water until neutral pH was achieved. Finally, the samples were dried at 105°C for 12 hours. The remaining sample was the α-cellulose content of the sample. The measurement was repeated 5 times for each type of cellulose.

2.4 XRD Analysis

X ray Diffraction (XRD) analysis was carried out using a PANalytical X Ray diffractometer using a Cu-Kα source (λ = 0.154nm) with a 2θ range of 5 – 30° with a scanning speed of 1°/minute.

2.5 Disintegration, Refining, and Microgrinding with SuperMassColloider

The fibrillation process for both celluloses of pulps was carried out in stages, and samples were collected at every stage to fabricate films with and characterize. First the pulps were disintegrated using a standard lab disintegrator (TMI, Rokonkoma, NY, USA) for 15,000 revolutions at a 10% consistency. Subsequently the pulps were refined in a PFI (TMI, Amityville, NY, USA) mill for 20,000 revolutions.

After PFI refining, microgrinding was done using a SMC (SuperMassColloider, MKZA6-2, Masuko Sangyo Co. Ltd, Japan) at 1500 rpm. The SMC consists of two stone discs grinding pulp between them, with a certain gap in between which can be adjusted based on degree of fibrillation required. The discs were set at a gap of -100µm which represents a negative setting; however, the constant presence of pulp ensures no direct contact between the discs and high degree of fibrillation of the pulp. Pulp was fed continuously through the SMC and samples were removed periodically for analysis.

2.6 Fabrication of Films from pulp

The pulps produced from the four different stages, disintegration, PFI refining, 20 passes through SMC, and 60 passes through SMC were used to fabricate films. All slurries were diluted to 1% to fabricate films via an ultrafiltration process. Millipore polyvinylidene difluoride (PVDF) membranes of diameter 142mm and a pore size of 0.22µm were used. After the slurries were dewatered with the ultrafiltration apparatus they were placed between smooth metal caul plates and then between three sheets of blotter paper, and compressed at a load of 60psi to remove any excess water. Subsequently the films were dried in a flatbed dryer under approximately 20psi load and 50°C for 24 hours. Multiple films were made for each type of pulp.

2.7 Characterization of films

After fabrication the films were characterized for physical dimensions, contact angle, mechanical properties, thermal analysis and SEM imaging of the fracture surface of mechanically tested films to ascertain the morphology of fibers and nature of the boding between fibers.

Firstly, films were cut into discs of 47mm diameter with a disc cutter. Three discs were cut and weighed, and for every disc five measurements of thickness were made, and thus film grammage could be ascertained. For mechanical testing, a standard ASTM dogbone D-1708 was used and 4 samples for each type of film were tested in an Instron Bluehill II machine for measuring the mechanical strength of films.

To measure contact angle, films were taped onto glass slides to create a flat surface then a 5µl drop of water was carefully placed on top of the films surface for 5 minutes. Five measurements were made for each type of film sample. Contact angle was measured using a First Ten Angstrom goniometer, and the results were analyzed using FTA32 image processing software.

UV Vis measurements were performed in the range 300-800nm with an Agilent UV-Vis instrument.

Morphology of the fibers and fracture surface was analyzed by SEM (LEO 1530 SEM, Carl Zeiss) at 5kV. The fracture surface samples were mounted vertically on SEM stages, whereas the fiber samples were prepared by air drying a drop of fiber suspension on an SEM stage and gold

sputtering (Quorum 150ES) for 60 seconds. Thermal analysis was performed in a Perkin Elmer TGA from 25°C – 500°C at a rate of 10°C/min under a nitrogen atmosphere.

3. Results and Discussion

3.1 α – Cellulose Quantification

α - Cellulose content can help quantify the purity of both cellulose I and II. By using the method described, almost all the hemicelluloses can be removed from the cellulose samples. This gives insight into the pure cellulose and hemicelluloses contents of the samples. By comparing this for the pure samples, we can indirectly gain insight into the removal of hemicelluloses during the initial mercerization process. Shown in table (**1**) is the α-cellulose content of the native and mercerized cellulose. The α - cellulose content of the native cellulose and the mercerized cellulose were about 84%, and 95% respectively. The residue is mainly thought to be hemicelluloses which are removed due to the high alkali concentration. The mercerized cellulose showed a much higher α - cellulose content since they had already been through the mercerization process and most of the hemicelluloses were removed during that process.

3.2 SEM: Fiber Morphology

SEM images of individual fiber surface before and after mercerization are shown in figure (**1**). Cellulose-I fibers before mercerization show a flat morphology with some small fibrils visible on the surface. Cellulose-II fibers on the other hand have a smoother, cylindrical morphology and show aggregation of surface fibrils on the surface of the fibers. This aggregation of fibrils is due to the formation of stronger bonds between fibrils during the mercerization process [15, 17, 19].

3.3 XRD Analysis

The mercerization of the cellulose-I fibers was also confirmed via XRD analysis shown in figure (**2**). Both materials showed high degree of purity indicated by absence of any extraneous peaks. Cellulose-I fibers showed characteristic peaks at approximately 16° and 23°, which are typical for cellulose-I. Mercerized cellulose-I fibers showed characteristic peaks at approximately 12.6°, and a doublet of peaks at 20.2°, and 22°. The conversion of the singlet peak to the doublet are characteristic of mercerization of cellulose-I [15, 17, 19]. Wang et al also studied the mercerization of cellulose I for the purpose of conversion to cellulose II nano fibers, and obtained similar characteristics of XRD patterns of the mercerized cellulose. Yue et al studied the properties of freeze dried cellulose nano crystals (CNCs) CNC-I and CNC-II, and found that the change of singlet to doublet peak signifies the change of crystallites from the 200 plane in CNC-I to 110 and 200 planes.

Shown in figure (**3**) are typical XRD patterns obtained for films made from cellulose I and the mercerized fibers at different stages of fibrillation. The patterns obtained are very similar to the staring materials shown in figure (**2**) indicating that the micro grinding process does not

significantly change the crystalline structure of the materials in either case. Some reduction in crystallinity index are however expected due to the constant shear in the micro grinder, for a more detailed treatment of the changes in crystallinity due to fibrillation the reader is referred to Nair et al.

3.4 Physical Properties of Films

Films grammage, density and contact angle measurements are shown in table (**2**). Film grammage was measured to make sure that the films were of similar dimensions and were comparable in nature. Film grammage showed to be highly consistent for both celluloses of materials and across the different degrees of fibrillation. Consistent grammage was obtained by the fabrication process used where the mat formation, compression, and compressed drying processes are highly uniform[7, 8] . The target for grammage was 40g/m^2, while the films are close to the target grammage some variability is observed. This is clearly due to some fiber losses during the film formation process. Generally speaking, density also increased at every stage, except for cellulose I fibrils at the last stage. This is most likely due to a larger degree of fibril loss than earlier stages since the fibrils at this stage, as will be observed from the SEM images subsequently, have been fibrillated to diameter in the 10-100nm scale and are lost easily during the filtration process.

Contact angles were measured to provide an estimate of the wettability of the films made from different fiber celluloses. Generally speaking with increasing refining and fibrillation of cellulose fibers, films become increasingly dense and lose porosity. This is due to stronger hydrogen bonding between fibrils which agglomerate to fill the interstitial pore space in the fiber network. This phenomenon leads to an increase in the surface contact angle. Contact angle for films made from the two materials evolved very differently for the two materials with increasing fibrillation stages. Cellulose-I fiber films show some contact angle from the first stage, whereas cellulose-II fiber films show that the water wetting is too fast so the contact angle could not be measured until 60 passes in the SMC.

To observe the optical properties UV Vis measurements in the visible range were performed for all films. The spectra are shown in figure (**4**). The films were quite thick, in the order of 75 - 100μm and therefore the spectra obtained were quite noisy. However, in both cases of cellulose I and II films the spectra show a clear reduction of absorbance with increasing degree of fibrillation. In the case of cellulose I there is a clear reduction in the absorbance with every stage. On the other hand, in the case of cellulose II the disintegrated fiber and the PFI fiber films show a great degree of overlap in their spectrum. A reduction in absorbance is observed after 20 passes, and there is still some overlap observed in the 20 passes and 60 passes films. By observing the physical images and the SEM images of the surface of the films, these results become much clearer.

In the case of cellulose-I fibers, every stage induced an increasing degree of fibrillation. Whereas for cellulose-II fibers the fibrillation was limited until the very last stage due to initial agglomeration of fibrils resulting in poor bonding between fibrils and porosity for films. Due to the ease of fibrillation of cellulose-I fibers as observed in SEM images in figures (**5**), at every stage the films formed were structurally denser and showed an increase in contact angle whereas cellulose-II fibers did not. However in the case of cellulose-II fibers due to initial agglomeration of fibrils on the surface of fibers fibrillation was limited at every stage. Due to the difficulty of fibrillation, cellulose-II films were porous until 60 passes in SMC as observed in the cross section SEM images, and therefore the water wetted the film too fast so the contact angle for the films could not be measured until 60 passes in SMC [26, 27].

Figure (**5**) shows images of films made from cellulose-I fibers and SEM images of corresponding fibers at different degrees of fibrillation. Cellulose-I fiber films show a simple progression of decrease in opacity at every fibrillation stage, due to ease of fibrillation and decrease in fiber size at every stage. Films made from fibers after PFI refining films are significantly more translucent than just disintegrated fiber films, figures **(5 (a, b))** correspondingly show the reduction of fiber size. In figure (**5a**), large fibers with cross section of tens of microns are visible and after PFI refining (figure (**5b)**), fibers show a significant reduction in size, and submicron sized fibers are visible. After 20 passes in the SMC (figure (**5c**)), fibers with diameters of the order of hundreds of nanometers are visible. Finally after 60 passes in SMC, fibers with diameters of few nanometers are visible (figure (**5d**)). The SEM images in figures (**5 (a, b, c, d**)) shows a decreasing fiber size at every stage of fibrillation for which correlates well with decreasing opacity of films [28].

Figure (**6**) shows images of films made from cellulose-II fibers and SEM images of corresponding fibers at different degrees of fibrillation. Cellulose-II fiber films showed a much different progression than cellulose-I fiber films. They initially displayed some translucence but this is because there is significant porosity in the film structure due to poor bonding between fibers. The SEM image in figure (**6a**) shows the structure of disintegrated cellulose-II fibers, which are smooth and display no surface fibrillation. This lack of surface fibrillation would cause porosity in the films due to lack of inter fiber bonding. After PFI refining (figure (**6b**)), the fibers showed some increase in fibrillation but no decrease in fiber size, causing only the inter fiber bonding to slightly improve. This resulted in the films being more opaque than the last stage, even though some porosity in the films is observable. After microgrinding for 20 passes, the films still showed limited reduction in opacity to the PFI refined fiber films due to no limited reduction in fiber size. In the SEM images it was observed that fibers of cross section of few microns were visible, and few submicron sized fibers were visible. Only after microgrinding for 60 passes, the films showed a significant decrease in opacity as compared to the previous stages. SEM image in figures (**6d)** shows that finally after 60 passes in SMC there is significant reduction in size of fibers down to the submicron level, and films show a reduction in opacity [28].

3.5 Mechanical Properties of films

We attempted to obtain similar grammage for the films, and as shown earlier, the grammage was maintained to be as consistent as experimentally possible. However, it was also observed that the density of the films increased with increasing degree of fibrillation. This is expected as the fibers become smaller, they form a better packed structure, which is higher in density. Increased density will in turn translate to better mechanical performance due to better entanglement of fibers and higher specific bonding between the fibers.

Figure (**7**) displays typical stress strain curves obtained for cellulose-I and II fiber films made at different degrees of fibrillation. Table (**3**) shows the mean of 4 observations. The fracture cross section of the mechanically tested films was analyzed by SEM imaging, shown in figures (**8-11**). This gave us the opportunity to observe the cross section of the films, the breaking mechanism, fiber size, and degree of fibrillation at different stages. Generally speaking, greater degree of fibrillation leads to increased mechanical strength [29-31]. This increase is directly related to the increase in exposed surface area of micro fibrils on the surface of fibers, which leads in turn to increased bonding strength per until area [31]. The break at ultimate tensile stress in highly bonded films is observed because these bonds act in unison under strain until failure is reached [15, 31].

In figure (**8**), the SEM images of the cross sections of films made from disintegrated fibers show that these fibers are very long and have large diameters in the orders of tens of microns. The two types of fibers show very different morphology as well. Cellulose-I fibers have a flat cross section with some fibrillation on the surface visible, whereas cellulose-II fibers show a smoother more cylindrical cross section [15, 17, 29, 31]. No break in the fiber morphology is observed in these images and long entangled fibers can be clearly seen, implying that the fibers are merely entangled with each other and there is no significant inter-fiber bonding. This results in the films displaying a tear behavior rather than a break behavior under strain.

Figure (**9**) shows the morphology of cross section of films made from PFI refined fibers. After being refined in the PFI, both types of fibers show some changes in morphology. The cellulose-I fibers show a significant degree of fibrillation, and a heterogeneous morphology is observed. Large number of micron and submicron sized fibrils are now visible alongside much larger fibers [4, 29]. In the case of cellulose-II the larger fibers show change in shape from a cylindrical form to a more flat fiber structure with some surface fibrillation. This is typical when fibrillation is only limited to the fiber surface, and shearing forces flatten the surface [4].

Under strain, cellulose-I fiber films showed significant increase in mechanical strength, while cellulose-II fiber films still showed tear behavior. This can be attributed to the physical changes observed in the fiber morphology. The smaller fibrils visible in cellulose-I fibers allude to an increase in inter fiber bonding. Additionally, there was significant improvement in the density of the films' packing structure. Whereas cellulose-II fibers only showed minor fibrillation and still

displayed tear behavior indicating that inter fiber bonding was limited and the main film forming mechanism was still entanglement of fibers [4, 31].

Figure (**10**) shows the morphology of films made from fibers after 20 passes in SMC. After 20 passes in the SMC, both types of fibers show significant increase of mechanical strength. It is expected for the cellulose-I fiber films to show some increment due to the ease of fibrillation. Cellulose-II fiber films after this stage of fibrillation have evolved from a tear behavior to displaying a break at a defined tensile strain, rather than tearing apart while being strained. Cellulose-I fibers displayed a significant shift in fiber size, no large fibers are visible, and the structure is more homogeneous. Microgrinding has previously been shown to be very effective in converting cellulose-I fibers to micro fibrillated cellulose and is observed here as well[32]. For cellulose-II fibers, microgrinding has limited effect on the degree of fibrillation as indicated by the morphology of fibers. Fibrillation still seems to be hampered due to the initial aggregation of fibrils during the mercerization process[15]. However, these films were observed to show break at a defined stress under strain. This indicates that 20 passes in SMC has caused enough fibrillation to increase strength of the films by enhancing bonding between exposed fibrils[31].

Figure (**11**) shows the morphology of films made from fibers after 60 passes in SMC. After 60 passes in the SMC both celluloses of fibers showed a micro fibrillated structure. This also translated into significantly better mechanical properties for both celluloses of materials. Cellulose-I fibers do not display microfiber like morphology, but an almost amorphous polymer like structure, where individual fibrils cannot be observed even at the high magnification shown here. The films made from cellulose-I fibers show an extremely well packed dense structure. In the case of cellulose-II fibers, micro fibrils can now be observed and the films show a very well packed dense structure as well. However, these fibers are still very different in morphology from cellulose-I fibers. Cellulose-II fiber films now showed an average ultimate tensile stress of 75MPa, whereas cellulose-I showed an ultimate tensile stress of 135MPa.

3.6 Thermal Analysis

Thermogravimetric and derivative thermogravimetric analysis were performed to compare the differences in thermal degradation of films made from cellulose-I and II fibers at different levels of fibrillation. TGA and DTGA curves are shown in figure (**12**), maximum degradation temperatures and maximum rate of degradation are shown in table (**4**). Generally speaking, the degradation process for celluloses and hemicelluloses begins above 200°C, and any linked water also starts evaporating causing loss of mass. While the temperature is less than 200°C, there is some mass loss and limited degradation. The onset for degradation was observed in all the different fiber celluloses in approximately 300°C region. With increasing degree of fibrillation an increase in surface area occurs therefore thermal degradation is easier and a drop in maximum degradation temperature is expected.

For both cellulose-I and II fibers the behavior of disintegrated and PFI stage fibers is almost identical, with cellulose-II fibers displaying a lower maximum rate of degradation as compared to cellulose-I fibers. After 20 passes in the SMC the thermal behavior of the two cellulose types begins to differ markedly. Cellulose-I fibers show a significant drop in both maximum degradation temperature and the maximum rate of degradation from previous stages, whereas cellulose-II fibers show a minor shift from the previous stages. This is due to the differing degrees of fibrillation of the two celluloses. Cellulose-I fibers show a significant decrease in fibers size at this stage, where submicron sized fibrils are visible, whereas cellulose-II still shows large micron sized fibers. This difference clearly alludes to the fact that there is a large difference in the specific surface area of the two fibers at this stage. After 60 passes, cellulose-I fibers show further reduction in maximum degradation temperature, which is expected since an increased degree of fibrillation is observed in the fibers. Cellulose-II fibers on the other hand, show a large decrease from the previous stage. Cellulose-II displays this large difference because after 60 passes in SMC, a high degree of fibrillation has been induced as observed in the SEM images and film structure. This causes the maximum degradation temperature to drop indicating an increase in surface area of the fibers [29, 32].

4.0 Conclusions

Cellulose-I pulp was converted to cellulose-II by mercerization with a 20% NaOH solution. The success of conversion of cellulose-I to II via mercerization of was confirmed by α – cellulose content, XRD, and SEM analysis. α – cellulose content changed from 84% to 96% upon mercerization indicating loss of almost all hemicelluloses during mercerization. XRD analysis confirmed the change in arrangement of crystalline domains to an antiparallel arrangement typical of cellulose-II. SEM analysis of individual fibers shows a difference the arrangement of surface fibrils. Cellulose-I fibers were initially flat and had some micro fibrils visible on the surface, whereas cellulose-II fibers showed a smooth cylindrical morphology indicating aggregation of surface fibrils. Both types of fibers were subjected to increasing stages of fibrillation in the order: disintegration, PFI refining, microgrinding by 20 passes in SMC, and 60 passes in SMC. Films were made via ultrafiltration followed by hot press method and characterized from fibers of the different stages of fibrillation. The films obtained were found to be uniform in terms of grammage and thickness owing to the ultrafiltration, hot press method. However density displayed significant increase with increasing degree of fibrillation. This is expected due to better packing efficiency and bonding between smaller, higher surface area of fibrils.

The grammage of the films was approximately 35g/m^2. The target grammage was 40g/m^2, and the slightly lower grammage indicated some fiber loss during the fabrication process. The density of the films increased with increasing degree of fibrillation from about 180g/m^3 to 455g/m^3 for cellulose I and 95g/m^3 to 385g/m^3 for cellulose II. Cellulose I films showed some contact angle to begin with which increased at every stage (14° - 64°), whereas cellulose II films did not display a contact angle until the final stage of fibrillation. The films also showed

increasing strength and an evolution of tensile strength from initially displaying a tear behavior indicating poor bonding to typical micro fibrillated cellulose films behavior as the fibers became increasingly fibrillated. The ultimate tensile strength for cellulose changed from tear behavior with no defined break to 134.5MPa. While on the other hand, the same change for cellulose II was a maximum of 75.1MPa from tear behavior.

It was observed that cellulose-I fibers were significantly easier to fibrillate as compared to cellulose-II fibers. SEM images showed that cellulose-I fibers followed a pattern of increasing fibrillation and decreasing fiber size at every stage. While for cellulose-II fibers, disintegration and PFI refining produced almost no fibrillation, after 20 passes some fibrillation was observed and only after 60 passes were nanofibers observed. For cellulose-I fibers the fibrillation stages directly correlated with an increase in mechanical strength and films cross section density at every stage due to increased bonding strength between small fibrils with large surface area. For cellulose-II fibers, significant fibrillation was observed only after 20 passes in the SMC, and film properties showed improvement from then on.

References

1. I. Siró and D. Plackett, *Cellulose*, 2010, 17, 459-494.
2. M. Minelli, M. G. Baschetti, F. Doghieri, M. Ankerfors, T. Lindström, I. Siró and D. Plackett, *Journal of Membrane Science*, 2010, 358, 67-75.
3. X. Zhang, Z. Lin, B. Chen, W. Zhang, S. Sharma, W. Gu and Y. Deng, *Journal of Power Sources*, 2014, 246, 283-289.
4. S. S. Nair, S. Sharma, Y. Pu, Q. Sun, S. Pan, J. Y. Zhu, Y. Deng and A. J. Ragauskas, *ChemSusChem*, 2014, 7, 3513-3520.
5. H. Cai, S. Sharma, W. Liu, W. Mu, W. Liu, X. Zhang and Y. Deng, *Biomacromolecules*, 2014, 15, 2540-2547.
6. X. Zhang, Z. Lin, B. Chen, S. Sharma, C.-p. Wong, W. Zhang and Y. Deng, *Journal of Materials Chemistry A*, 2013, 1, 5835-5839.
7. H.-D. Huang, C.-Y. Liu, D. Li, Y.-H. Chen, G.-J. Zhong and Z.-M. Li, *Journal of Materials Chemistry A*, 2014, 2, 15853-15863.
8. M. Österberg, J. Vartiainen, J. Lucenius, U. Hippi, J. Seppälä, R. Serimaa and J. Laine, *ACS Applied Materials & Interfaces*, 2013, DOI: 10.1021/am401046x.
9. C.-N. Wu, T. Saito, S. Fujisawa, H. Fukuzumi and A. Isogai, *Biomacromolecules*, 2012, 13, 1927-1932.
10. K. Syverud and P. Stenius, *Cellulose*, 2009, 16, 75-85.
11. G. Rodionova, Ø. Eriksen and Ø. Gregersen, *Cellulose*, 2012, 19, 1115-1123.
12. H. Sehaqui, Q. Zhou, O. Ikkala and L. A. Berglund, *Biomacromolecules*, 2011, 12, 3638-3644.
13. A. Isogai, T. Saito and H. Fukuzumi, *Nanoscale*, 2011, 3, 71-85.
14. D. Roy, M. Semsarilar, J. T. Guthrie and S. Perrier, *Chemical Society Reviews*, 2009, 38, 2046-2064.
15. H. Wang, D. Li, H. Yano and K. Abe, *Cellulose*, 2014, 21, 1505-1515.
16. Y. Yue, C. Zhou, A. French, G. Xia, G. Han, Q. Wang and Q. Wu, *Cellulose*, 2012, 19, 1173-1187.
17. A. Sarko and R. Muggli, *Macromolecules*, 1974, 7, 486-494.
18. D. Klemm, B. Heublein, H.-P. Fink and A. Bohn, *Angewandte Chemie International Edition*, 2005, 44, 3358-3393.

19. E. Dinand, M. Vignon, H. Chanzy and L. Heux, *Cellulose*, 2002, 9, 7-18.
20. H. Shibazaki, S. Kuga and T. Okano, *Cellulose*, 1997, 4, 75-87.
21. L. A. Ramos, D. L. Morgado, F. Gessner, E. Frollini and O. A. El Seoud, *ARKIVOC: Online Journal of Organic Chemistry*, 2011, 416-425.
22. B. S. Kaith, A. S. Singha, S. Kumar and S. Kalia, *International Journal of Polymeric Materials*, 2008, 57, 54-72.
23. T. Isogai, M. Yanagisawa and A. Isogai, *Cellulose*, 2008, 15, 815-823.
24. M. Floros, L. Hojabri, E. Abraham, J. Jose, S. Thomas, L. Pothan, A. L. Leao and S. Narine, *Polymer Degradation and Stability*, 2012, 97, 1970-1978.
25. J. Zhu, X.-T. Dong, X.-L. Wang and Y.-Z. Wang, *Carbohydrate Polymers*, 2010, 80, 350-359.
26. L. Li, V. Breedveld and D. W. Hess, *ACS Applied Materials & Interfaces*, 2013, 5, 5381-5386.
27. B. Balu, V. Breedveld and D. W. Hess, *Langmuir*, 2008, 24, 4785-4790.
28. I. Siró, D. Plackett, M. Hedenqvist, M. Ankerfors and T. Lindström, *Journal of Applied Polymer Science*, 2011, 119, 2652-2660.
29. S. Nair, J. Y. Zhu, Y. Deng and A. Ragauskas, *Journal of Nanoparticle Research*, 2014, 16, 1-10.
30. A. N. Nakagaito and H. Yano, *Appl Phys A*, 2005, 80, 155-159.
31. W. Stelte and A. R. Sanadi, *Industrial & Engineering Chemistry Research*, 2009, 48, 11211-11219.
32. K. Abe, S. Iwamoto and H. Yano, *Biomacromolecules*, 2007, 8, 3276-3278.

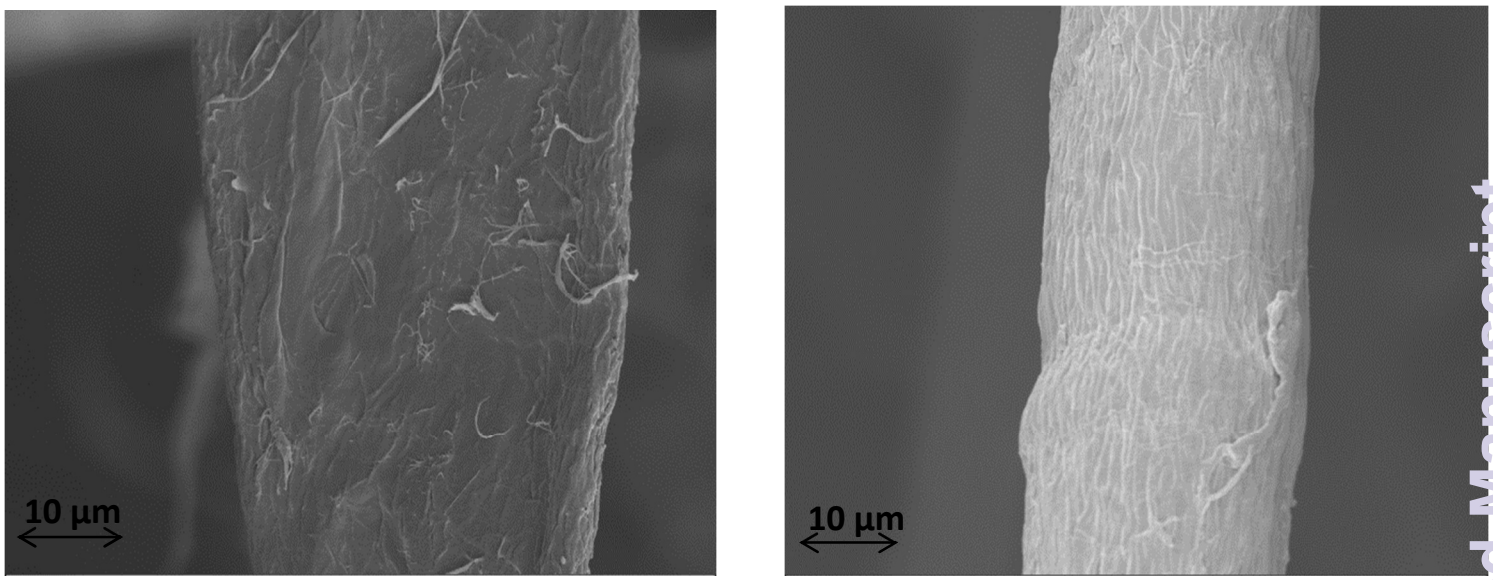

Figure 1: Cellulose I Fiber (left), Mercerized Cellulose Fiber (left)

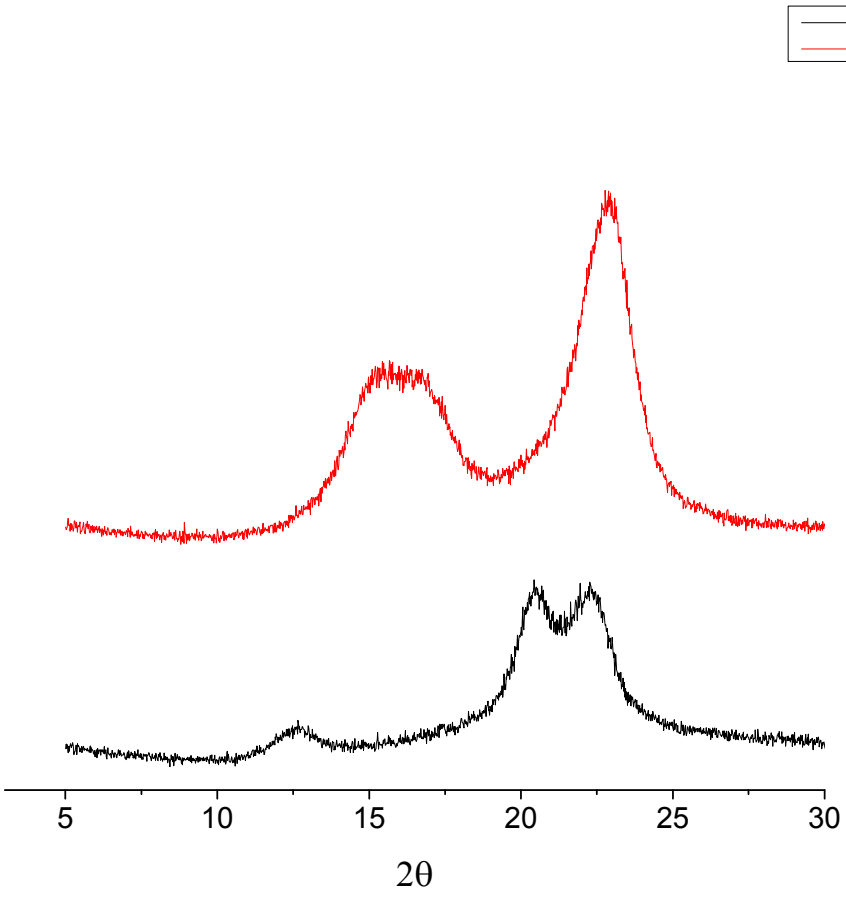

Figure 2: XRD Analysis: Cellulose and Mercerized Cellulose

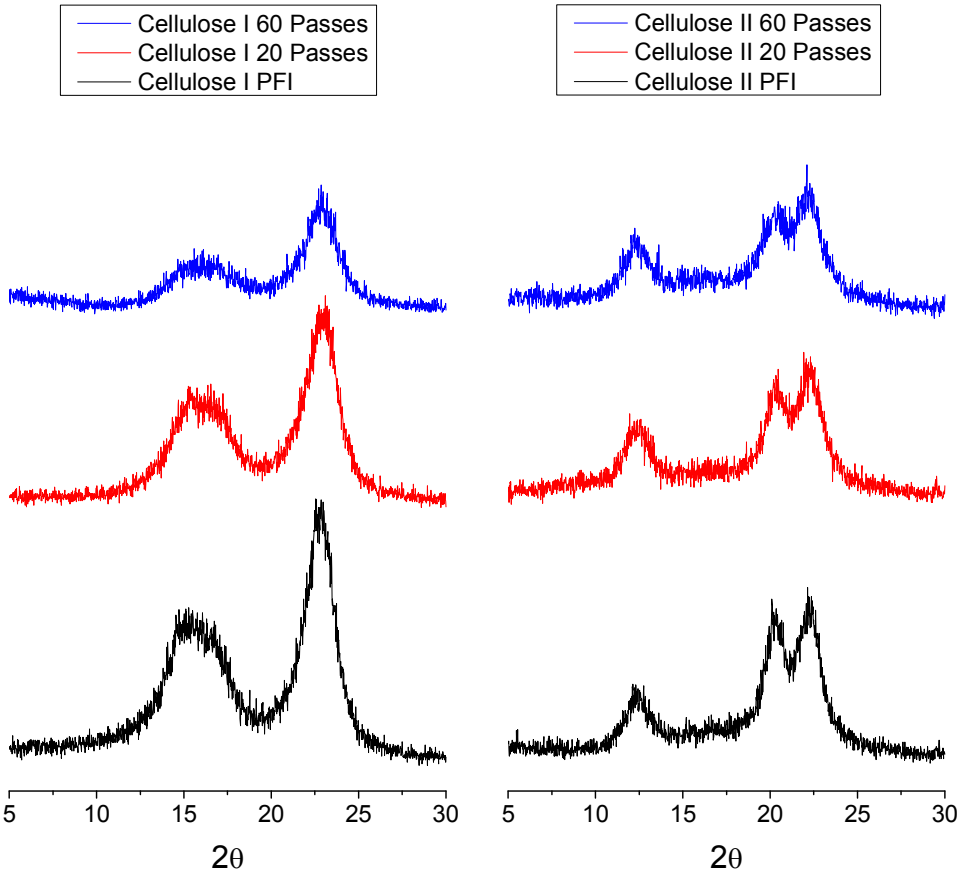

Figure 3: XRD Analysis of films

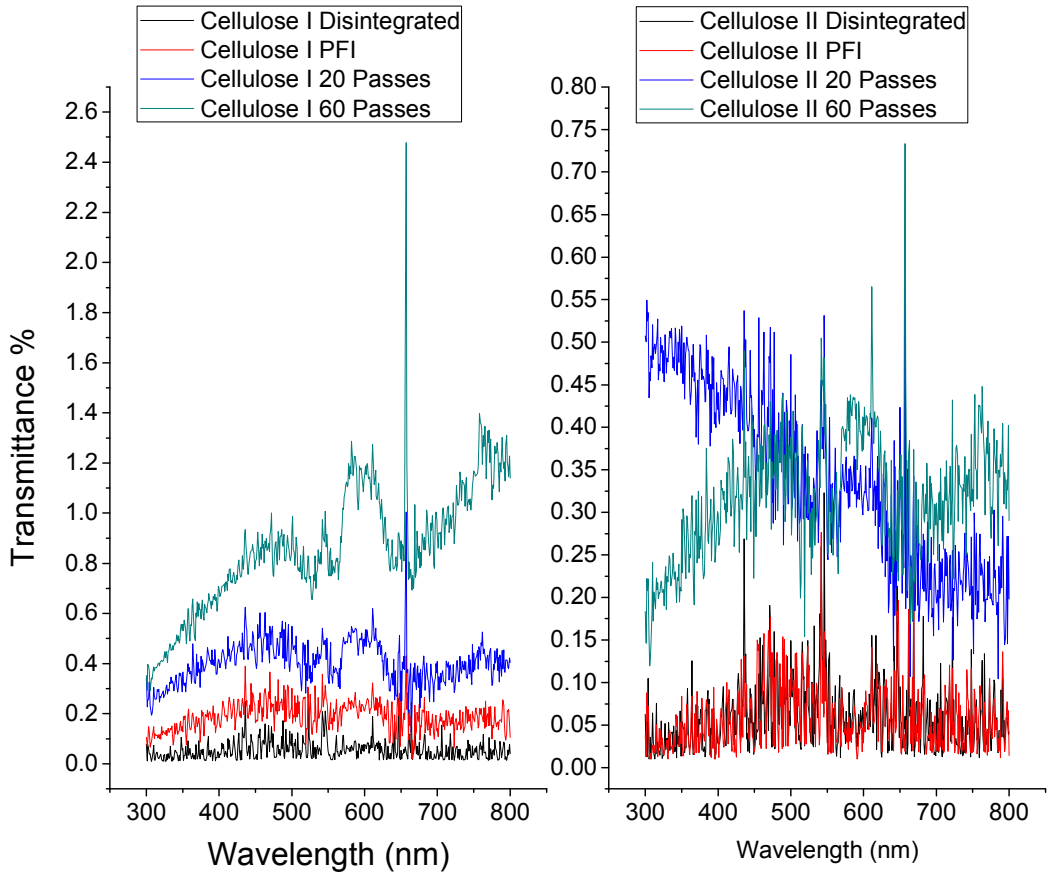

Figure 4: UV Vis Spectra

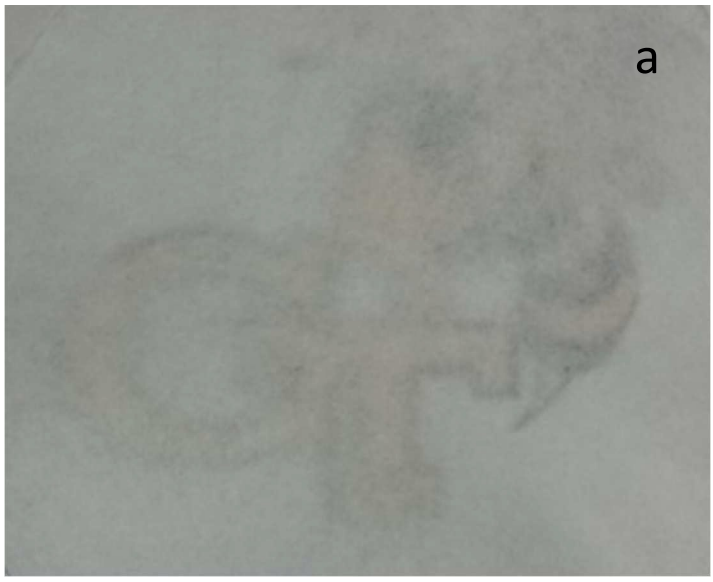

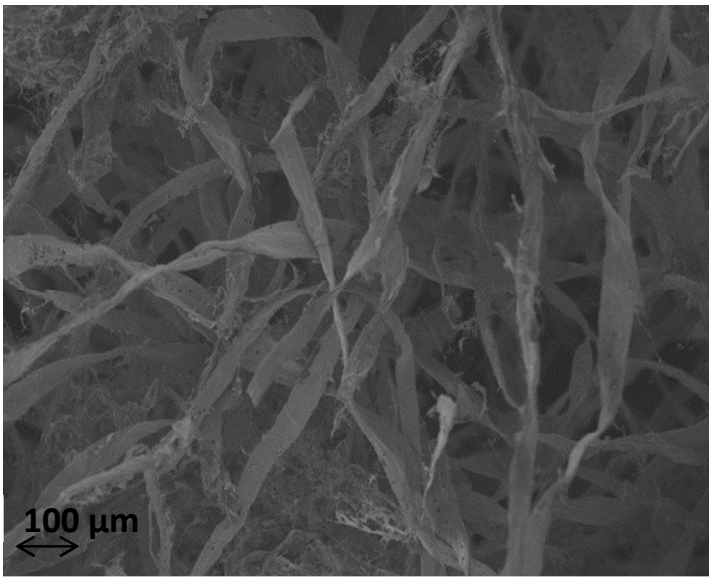

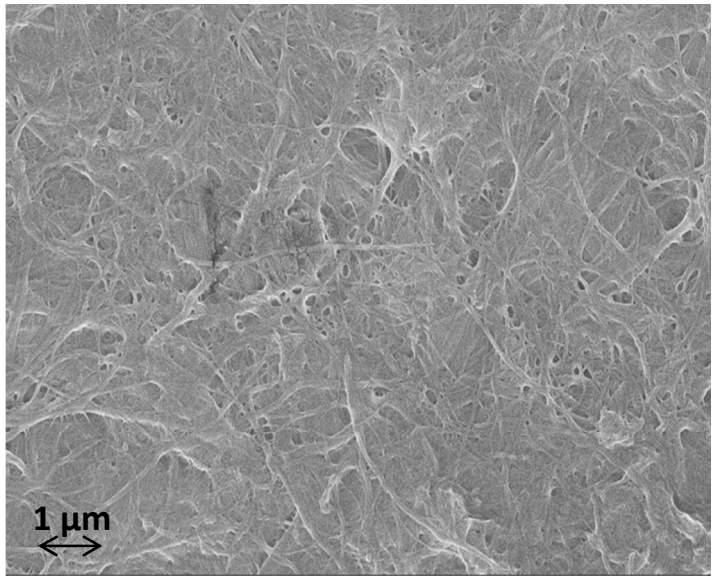

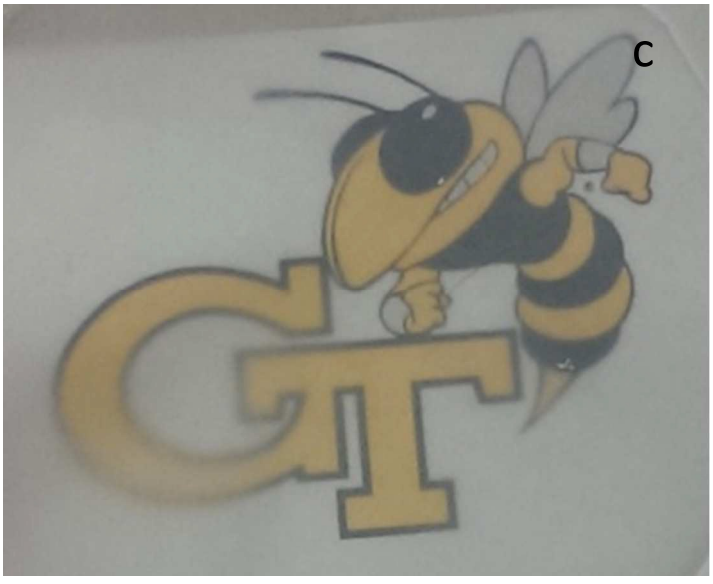

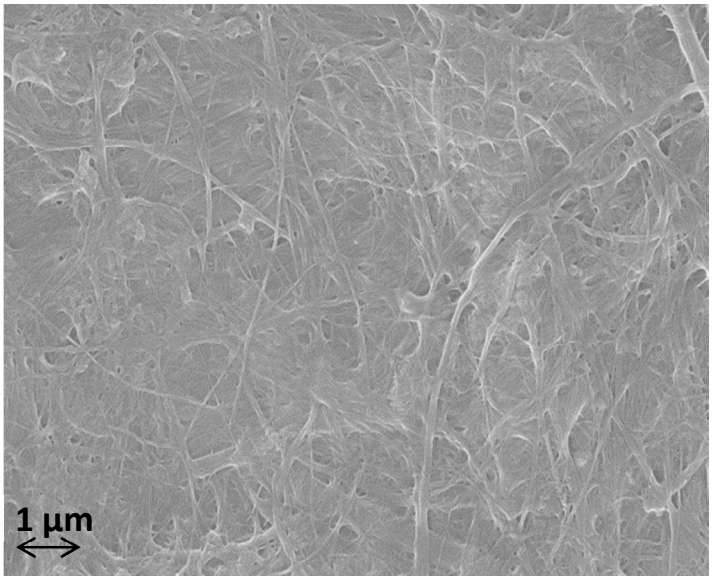

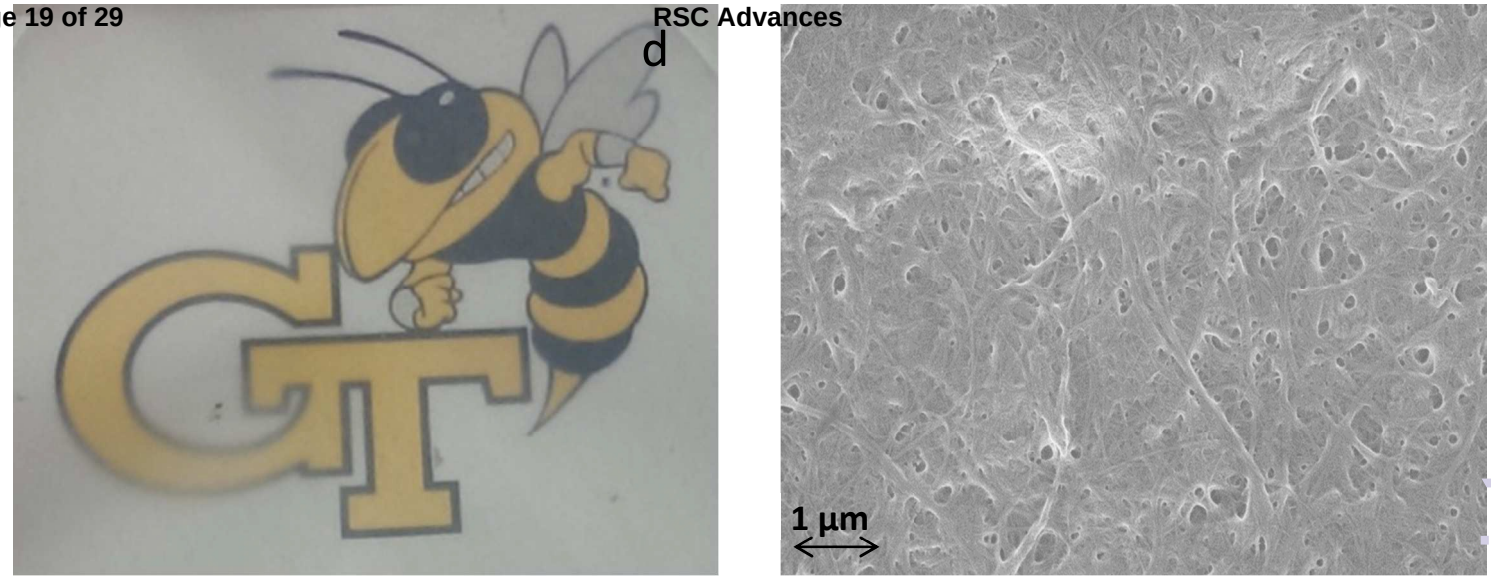

Figure 5: Cellulose I Films and Fiber SEMs (a. Disintegrated, b.PFI, c.20 Passes in SMC, d.60 Passes in SMC)

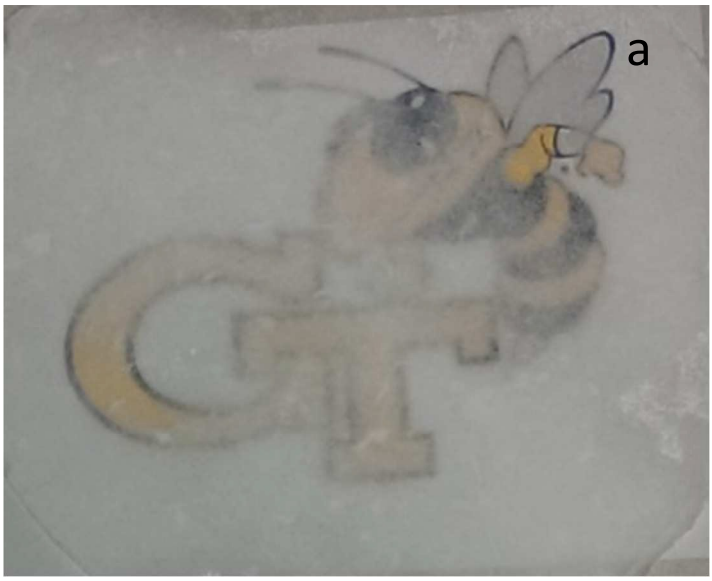

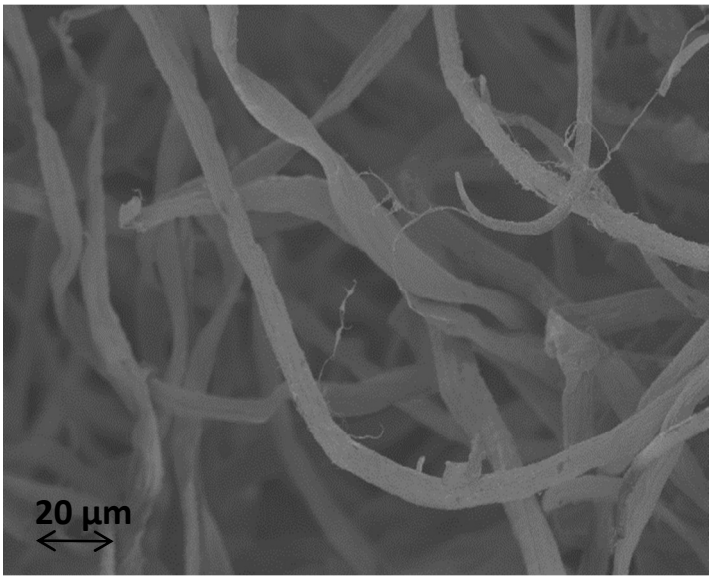

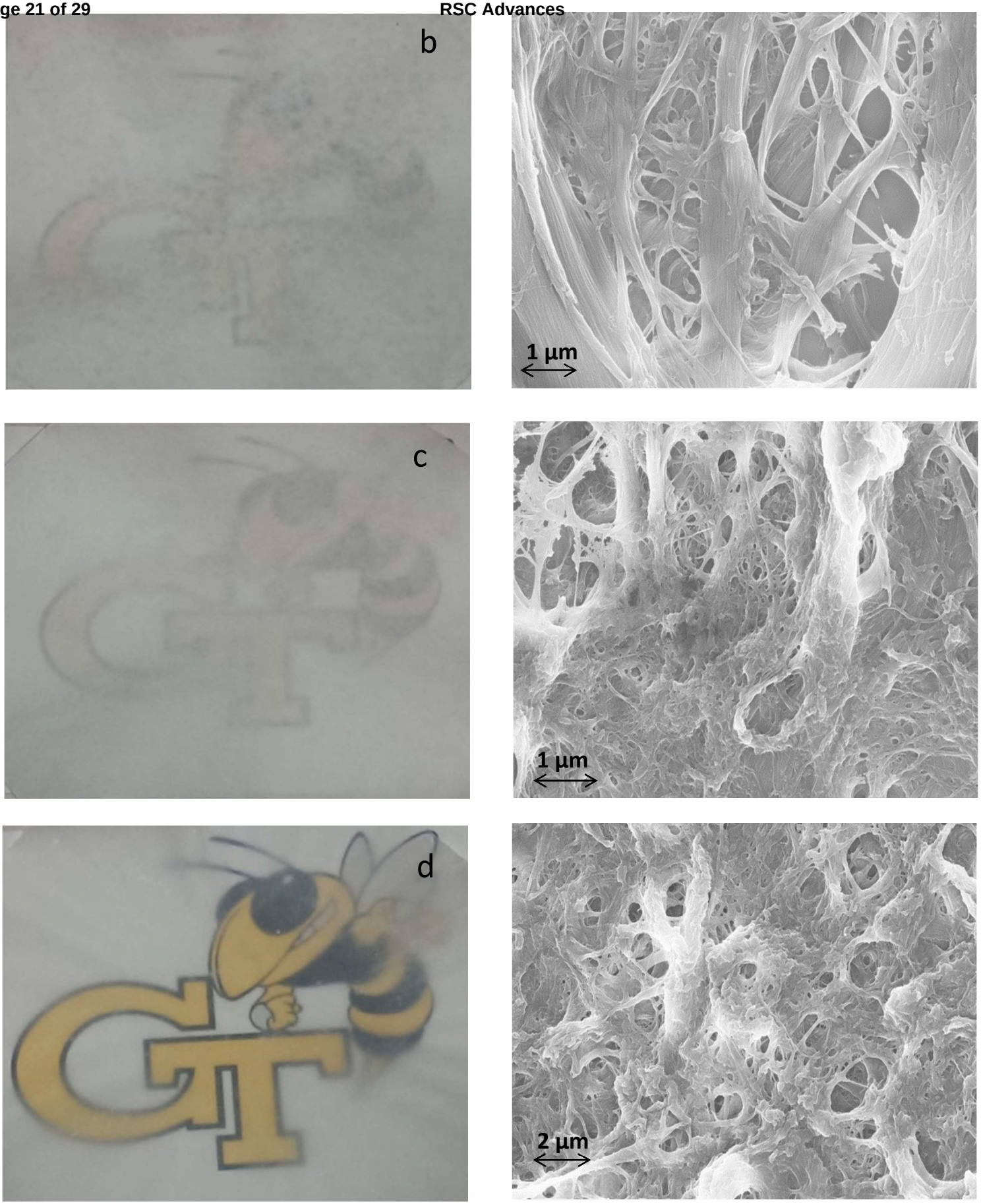

Figure 6: Cellulose II Films and Fiber SEMs (a. Disintegrated, b.PFI, c.20 Passes in SMC, d.60 Passes in SMC)

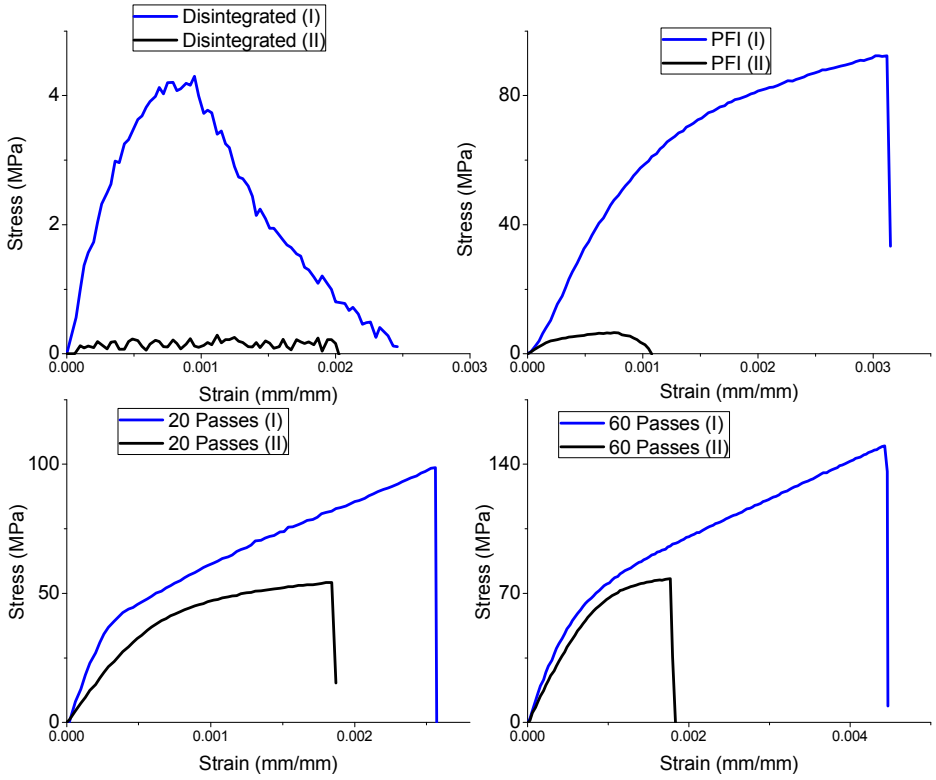

Figure 7: Typical Stress - Strain curves

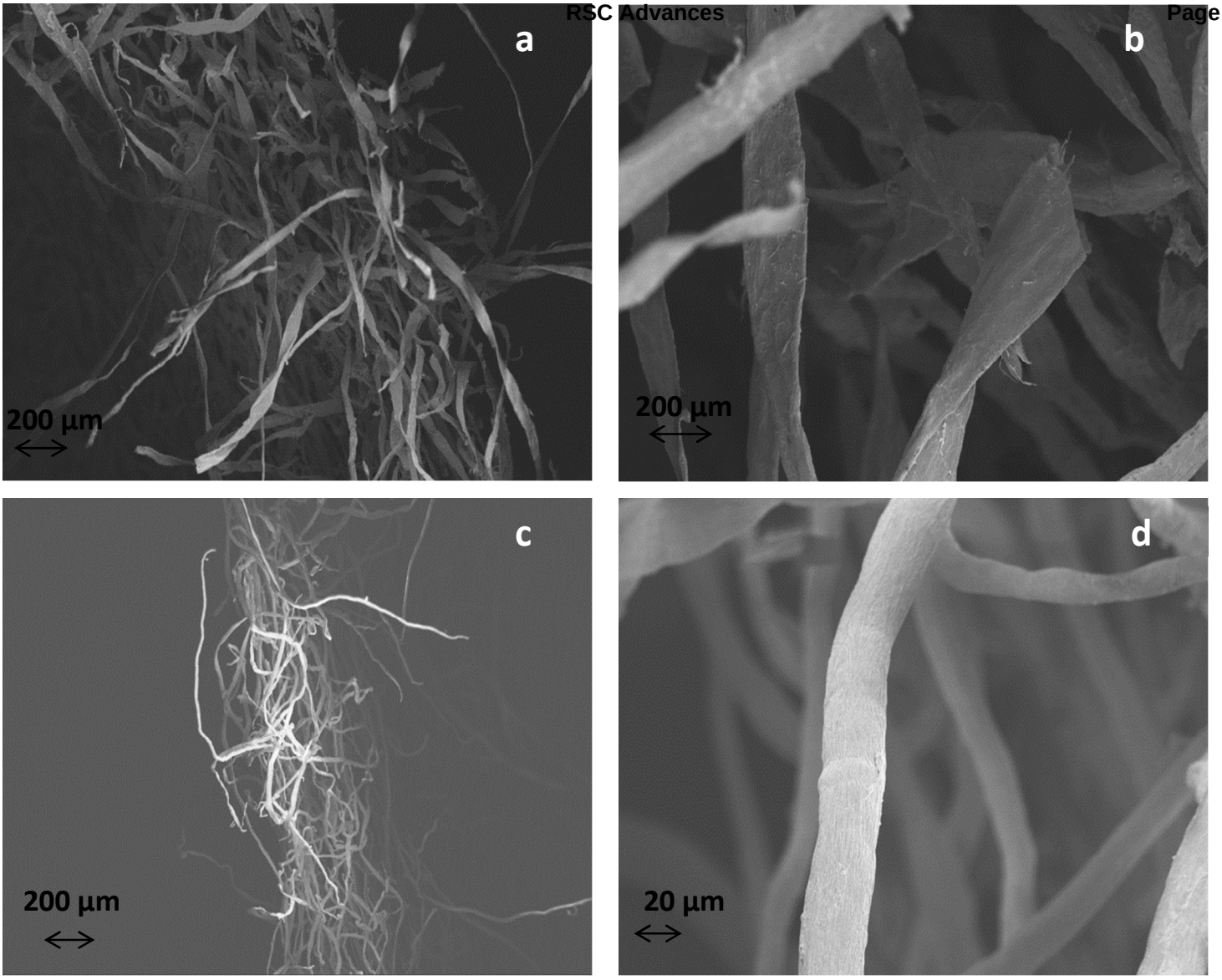

Figure 8: (a, b): Cellulose I Disintegrated Fibers, (c ,d): Cellulose II Disintegrated Fibers

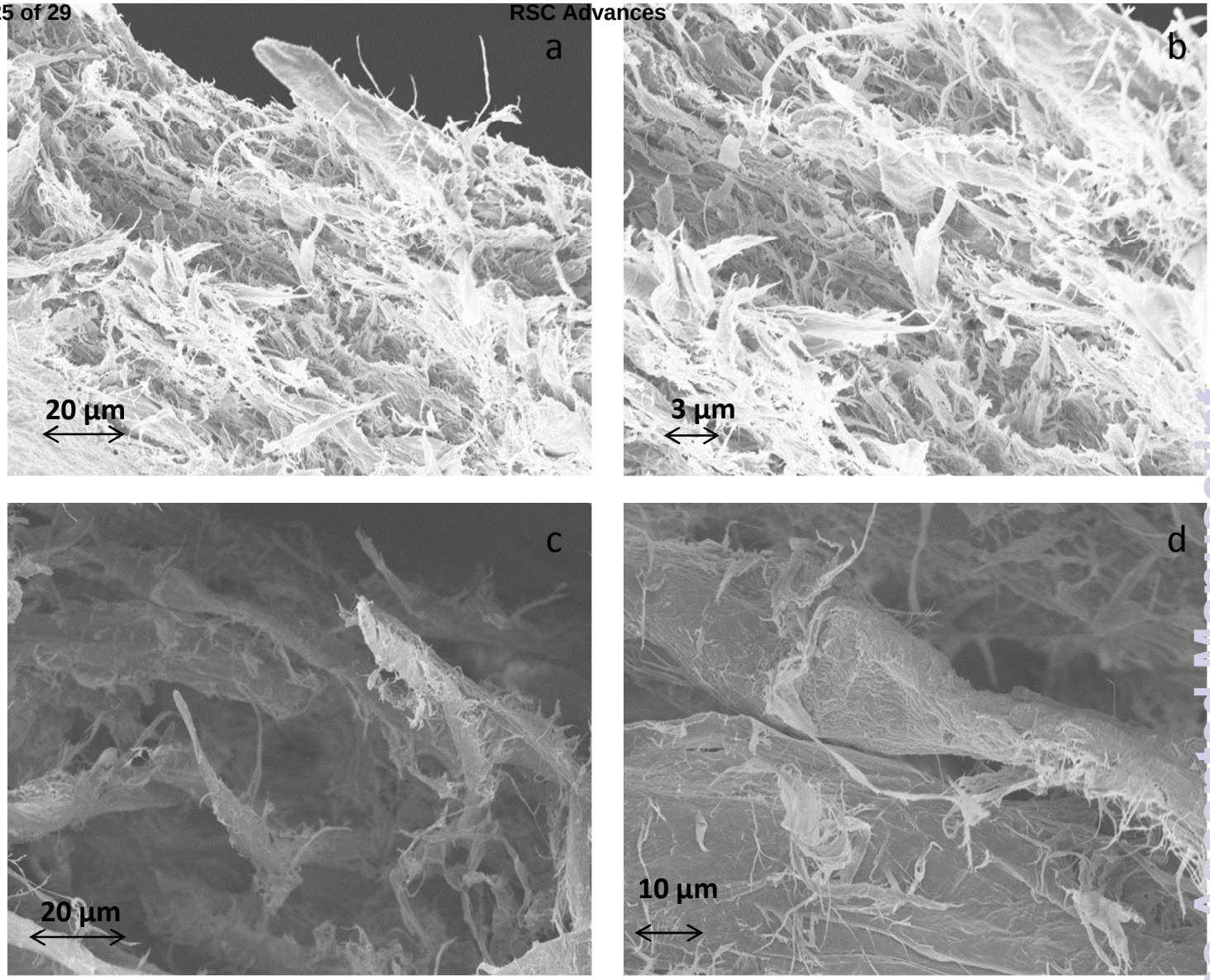

Figure 9: (a, b): Cellulose I PFI Fibers, (c ,d): Cellulose II PFI Fibers

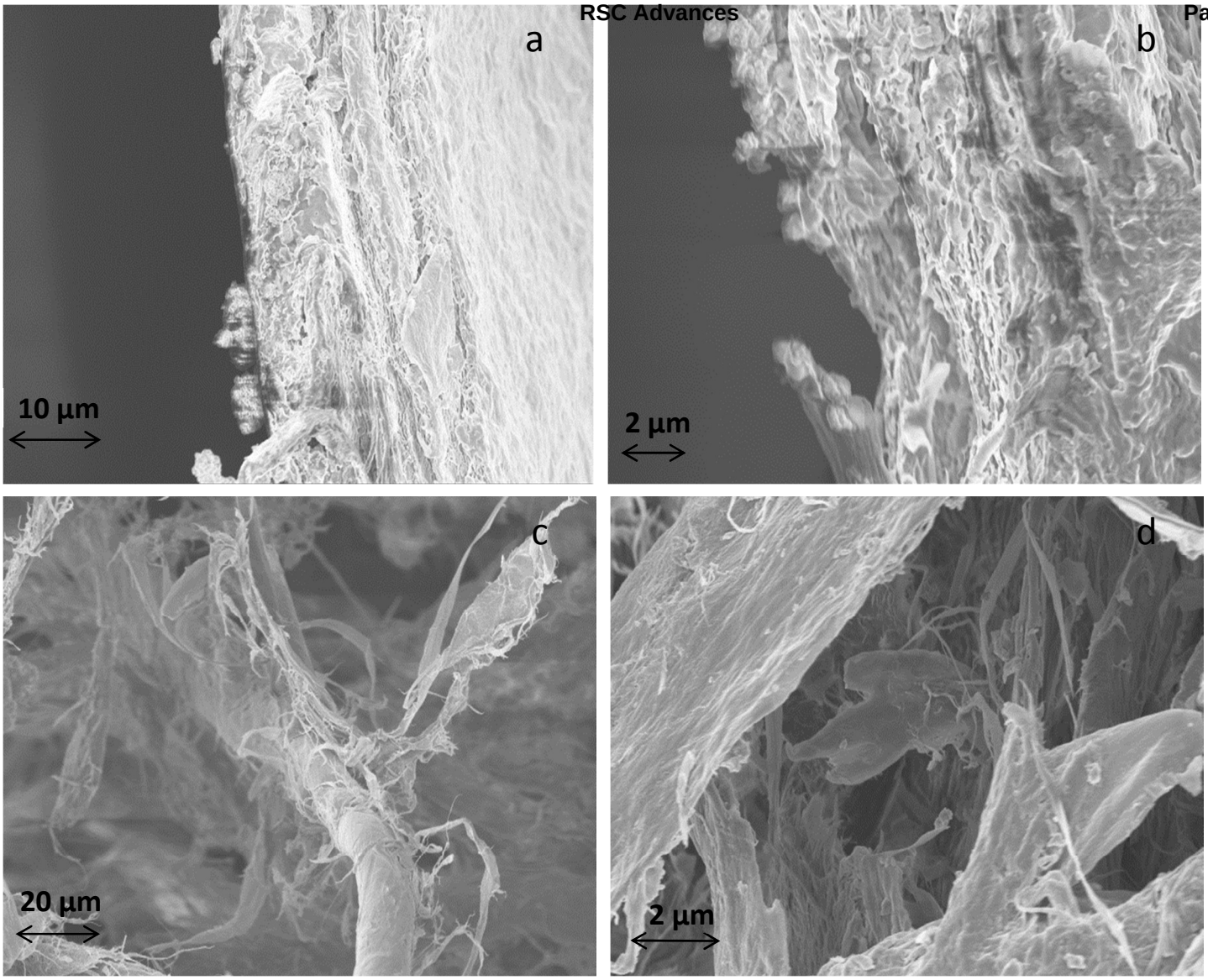

Figure 10: (a, b): Cellulose I 20 Passes in SMC Fibers, (c ,d): Cellulose II 20 Passes in SMC Fibers

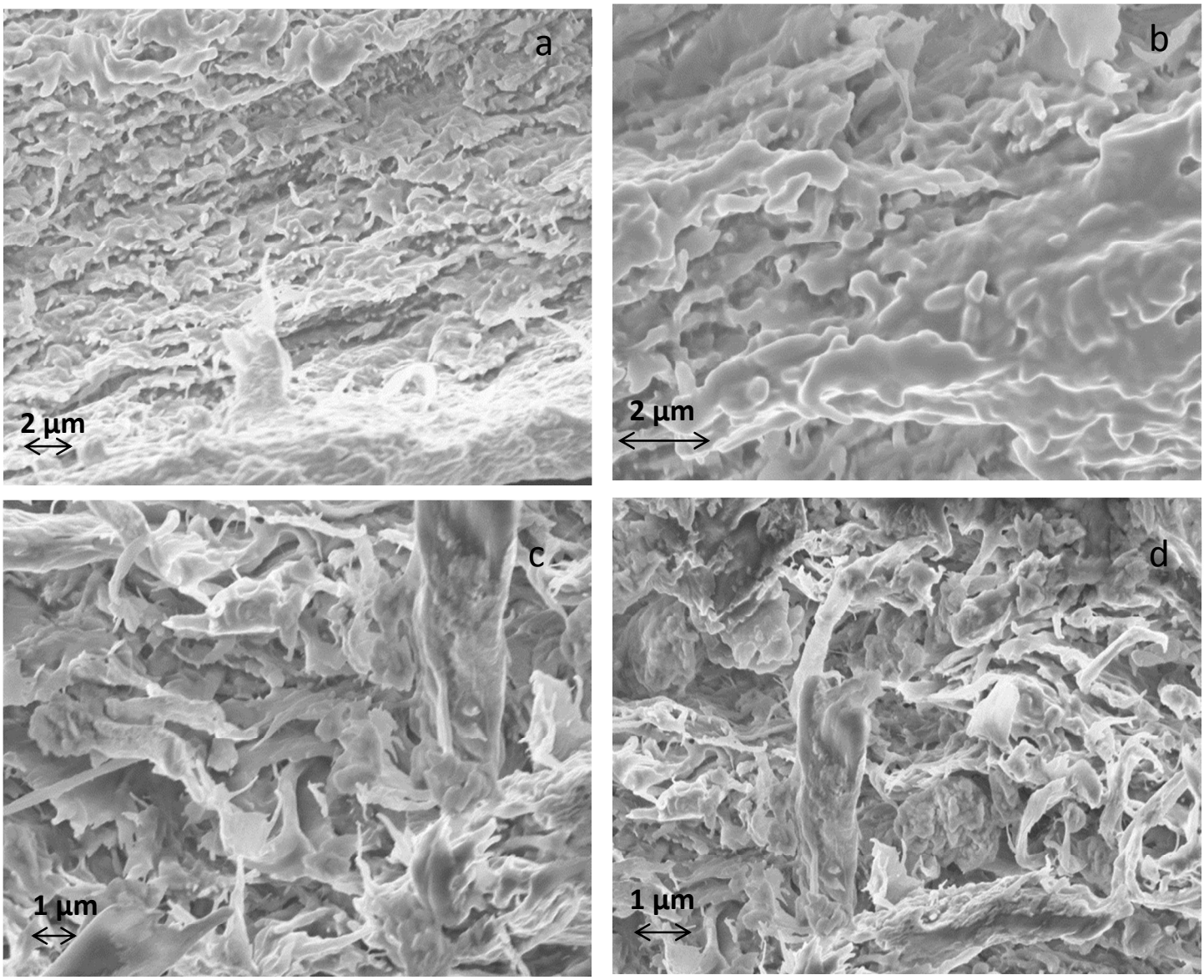

Figure 11:(a, b): Cellulose I 60 Passes in SMC Fibers, (c ,d): Cellulose II 60 Passes in SMC Fibers

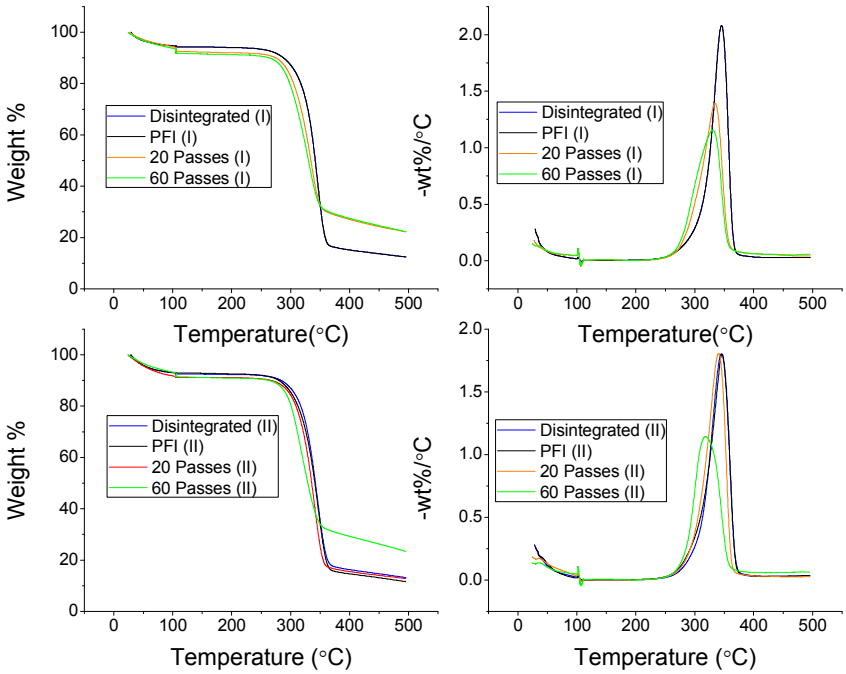

Figure 12: TGA / DTG Analysis

Table 1: α - Cellulose Content of native and mercerized pulp

Sample	Cellulose I	Cellulose II
α - Cellulose Content (g/g dry sample)	0.84±0.02	0.96±0.03

Table 2: Physical Properties of Films

	Sample	Disintegrated	PFI	20 Passes	60 Passes
Film grammage	**Cellulose-I (g/m^2)**	34.2±1.2	38.3±1.5	37.6±0.3	34.1±0.6
	Cellulose-II(g/m^2)	37.8±1.3	39.5±0.7	36.5±0.8	39.1±1.4
Film Density	**Cellulose-I (g/m^3)**	181.9±6.3	376.9±14.7	447.9±7.8	455.5±3.6
	Cellulose-II(g/m^3)	95.4±3.2	311±5.5	312.3±6.8	384.8±13.7
Contact Angle	**Cellulose-I (°)**	14.4±0.3	58.17±0.6	63.1±0.6	64.2±0.5
	Cellulose-II (°)	Water wetting is too fast and the contact angle could not be measured	Water wetting is too fast and the contact angle could not be measured	Water wetting is too fast and the contact angle could not be measured	57.7±0.4

Table 3: Mechanical Properties of films

		Disintegrated	PFI	20 Passes	60 Passes
Cellulose-I	**Strain at Break (mm/mm)**	-	0.0021	0.0024	0.0045
	UTS (MPa)	-	75.7	96.7	134.5
Cellulose-II	**Strain at Break (mm/mm)**	-	-	0.0015	0.0016
	UTS (MPa)	-	-	41	75.1

Table 4: Thermal Properties

		Disintegrated	PFI	20 Passes	60 Passes
Cellulose-I	**Max Thermal Degdration (°C)**	347	347	335	329
	Max Rate of Degdradation (-wt% / °C)	2.04	2	1.39	1.15
Cellulose-II	**Max Thermal Degdration (°C)**	346	345	340	316
	Max Rate of Degdradation (-wt% / °C)	1.81	1.8	1.8	1.14